Taylor & Francis
Taylor & Francis Group

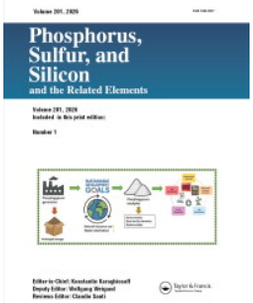

Phosphorus, Sulfur, and Silicon and the Related Elements

ISSN: 1042-6507 (Print) 1563-5325 (Online) Journal homepage: www.tandfonline.com/journals/gpss20

Design and evaluation of amine-functionalized salicylic acid loaded hollow mesoporous silica nanoparticles for treatment of triple-negative breast cancer

Sureba Sukumaran, Jyothi Kanagaraj, Mohana Priya, Priya Rajan & Azar Zochedh

To cite this article: Sureba Sukumaran, Jyothi Kanagaraj, Mohana Priya, Priya Rajan & Azar Zochedh (09 Feb 2026): Design and evaluation of amine-functionalized salicylic acid loaded hollow mesoporous silica nanoparticles for treatment of triple-negative breast cancer, Phosphorus, Sulfur, and Silicon and the Related Elements, DOI: 10.1080/10426507.2026.2627230

To link to this article: https://doi.org/10.1080/10426507.2026.2627230

Published online: 09 Feb 2026.

PHOSPHORUS, SULFUR, AND SILICON AND THE RELATED ELEMENTS
https://doi.org/10.1080/10426507.2026.2627230

Design and evaluation of amine-functionalized salicylic acid loaded hollow mesoporous silica nanoparticles for treatment of triple-negative breast cancer

Sureba Sukumaran[a], Jyothi Kanagaraj[b], Mohana Priya[c,d], Priya Rajan[c], and Azar Zochedh[e]

[a]Faculty of Health and Life Sciences, INTI International University, Nilai, Malaysia; [b]Department of Biotechnology, Kalasalingam Academy of Research and Education, Krishnankoil, India; [c]Department of Bioinformatics, School of Life Sciences, Vels Institute of Science Technology and Advanced Studies, Chennai, India; [d]Center for Research and Development, Biomaz Infosearch, Madurai, India; [e]Department of Computational Biology, Saveetha School of Engineering, Saveetha Institute of Medical and Technical Sciences (SIMATS), Saveetha University, Chennai, India

ABSTRACT

Triple-negative breast cancer (TNBC) is an aggressive and heterogeneous malignancy characterized by the absence of estrogen, progesterone, and HER2 receptors, limiting effective targeted treatment options. In this research, we investigated the anticancer activity of salicylic acid (Sa) encapsulated through hollow mesoporous silica nanospheres (HMSN). Molecular docking was initially done to assess the interaction of Sa with the major apoptotic and proliferative targets and found considerable binding affinities that imply anticancer activity. In accordance with these *in silico* results, Sa was encapsulated into HMSN effectively to produce Sa@HMSN, and the formulation was characterized for physicochemical properties using SEM, TEM, particle size, XRD, FTIR, Zeta potential, and BET analysis. An effective drug load and pH-dependent release mechanism was observed in HMSN. *In vitro* cytotoxicity was evaluated against MDA-MB-231 cells by MTT assay, exhibiting a dose-dependent inhibition of cell viability, with Sa@HMSN exhibiting significantly higher efficacy compared to free Sa or blank HMSN. Morphological observation revealed cellular shrinkage and membrane blebbing in treated cells. Ao/EtBr dual staining indicated apoptosis, with the Sa@HMSN treated cells showing chromatin condensation and nuclear fragmentation. Further, the expression of p53 was analyzed through immunocytochemistry. The findings indicate that Sa@HMSN are a promising nanotherapeutic platform for TNBC therapy, coupling predictive docking analysis with high *in vitro* efficacy.

ARTICLE HISTORY
Received 20 September 2025
Accepted 25 January 2026

KEYWORDS
TNBC cells; nano drug delivery; tumor suppressor p53; apoptosis; cytotoxicity

GRAPHICAL ABSTRACT

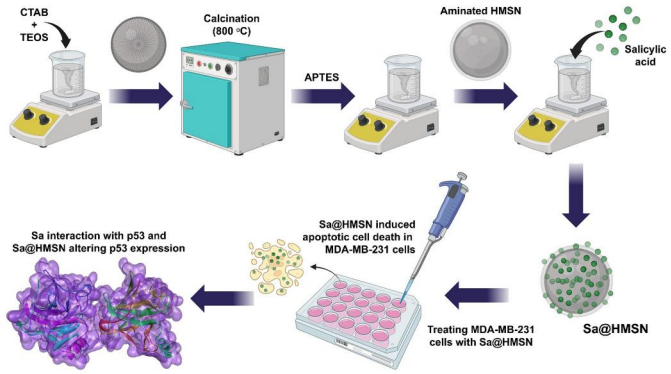

1. Introduction

Cancer remains one of the prevalent causes of morbidity and mortality globally, with breast cancer being the most common malignancy among females.[1] Breast cancer presents with about 2.3 million new cases and 685,000 deaths every year, as noted by GLOBOCAN 2020, a clear indication of an immense global health burden.[2] Although tremendous breakthroughs have been made in early detection and systemic treatments, breast cancer remains clinically problematic owing to its heterogeneity. Based on gene expression and receptor profiling, it is classified into a number of molecular subtypes, such as luminal A, luminal B, HER2-enriched, and triple-negative breast cancer (TNBC).[3] TNBC does not express estrogen receptor (ER), progesterone receptor (PR), or HER2, making it nonresponsive to existing hormonal or HER2-targeting therapies. TNBC constitutes about 15–20% of all breast cancers and is characterized by aggressive growth, early recurrence, high metastatic potential, and unfavorable prognosis.[4] Traditional chemotherapeutic drugs like anthracyclines and taxanes represent the backbone of TNBC treatment, but these agents are usually accompanied by systemic toxicity

CONTACT Azar Zochedh azar2411@gmail.com Department of Computational Biology, Saveetha University, Chennai, Tamil Nadu, 602105, India

and multidrug resistance.[5] Due to the unavailability of receptor-based therapeutic strategies, alternative methods urgently need to be developed to deliver therapeutic agents selectively to TNBC cells with minimal off-target effects.

In this regard, nanotechnology-based drug delivery systems (DDS) have emerged as a promising strategy for enhancing the selectivity, bioavailability, and therapeutic index of anticancer agents.[6] Among all the nanocarriers that have been designed, hollow mesoporous silica nanoparticles (HMSN) are notable for their distinct physicochemical characteristics of having a large surface area, adjustable pore size, and hollow interior to provide high drug loading and controlled release. HMSN also possess superior biocompatibility, chemical stability, and surface modifiability to make them very versatile for both passive and active targeting.[7] These characteristics are particularly useful for the delivery of hydrophobic and unstable drug molecules since HMSN are able to shield the cargo from premature degradation and enable release in accordance with internal stimuli like acidic pH.[8] Salicylic acid (Sa) is a phenolic compound that is naturally found in various sources and well recognized due to its anti-inflammatory and keratolytic activities. Salicylic acid is the active form of aspirin, and it has been used traditionally in dermatological and rheumatological treatments. Nonetheless, recent findings indicate that Sa also possesses broad-spectrum anticancer activity in the form of induction of apoptosis, cell proliferation inhibition, and metastasis suppression in different tumor models.[9] Aspirin's active metabolite Sa was chosen as a potential treatment because of its proven anti-inflammatory and anticancer qualities that are pertinent to triple-negative breast cancer (TNBC). Protumorigenic signaling pathways, including NF-κB and PI3K/Akt, which are often overexpressed in MDA-MB-231 cells leading to proliferation, invasion, and treatment resistance, are modulated by Sa and inhibited by cyclooxygenase-2 (COX-2). Salicylates and aspirin have been demonstrated in previous research to act as an inhibitor of cell viability, trigger apoptosis, and lessen the propensity for metastasis in TNBC models like MDA-MB-231 cells. Furthermore, salicylic acid's small molecular size and acceptable safety profile make it a good option for nano-delivery strategies meant to improve intracellular absorption and therapeutic efficacy in aggressive breast cancer subtypes.[10,11] Although having these encouraging properties, Sa's therapeutic application as an anticancer drug is hampered by its poor solubility in water, extensive metabolism, short half-life, and systemic toxicity at elevated doses.[12] This makes the finding of a DDS that is able to increase Sa's bioavailability and tumor-targeted delivery without compromising its pharmacological efficacy imperative. Incorporation of Sa into HMSN is a visionary approach toward overcoming these limitations. The inner hollow space of HMSN enables Sa encapsulation with high efficiency, while the mesoporous shell promotes prolonged and pH-responsive drug release in the acidic tumor environment.[13] In addition, HMSN surfaces can be easily functionalized with targeting ligands for enhanced uptake by cancer cells. Previous studies have shown successful encapsulation of anti-inflammatory drugs like curcumin, ibuprofen, and aspirin analogs in hollow mesoporous silica nanoparticles with improved cytotoxicity profiles and therapeutic outcomes.[14] Compared to solid silica, polymeric nanoparticles, and liposomes, hollow mesoporous silica nanoparticles (HMSN) have significant benefits over other nanoplatforms because of their special hollow core and mesoporous shell, which allow for extraordinarily high drug loading and effective encapsulation.[15] HMSN provide customizable and long-lasting drug release patterns by providing exact control over particle size, pore width, and shell thickness.[16] Compared to metal-based nanocarriers, HMSN are more versatile due to their wide surface area and abundance of silanol groups, which make surface functionalization with targeting or stimuli-responsive moieties simple.[17] Furthermore, HMSN overcome drawbacks like leakage and long-term toxicity seen in liposomal and metallic systems by demonstrating exceptional biocompatibility, minimal intrinsic toxicity, and improved structural stability under physiological settings.[18,19] However, the specific application of Sa-loaded HMSN (Sa@HMSN) in TNBC therapy remains underexplored. Even though nanocarrier systems for triple-negative breast cancer have been developed extensively, traditional platforms frequently have poor release control, restricted drug loading, and lack of selectivity for the aggressive tumor microenvironment. Furthermore, salicylic acid's therapeutic potential in TNBC is yet unexplored, especially in nano-enabled delivery systems intended for MDA-MB-231 cells. This study aims to fill that gap by formulating and characterizing Sa@HMSN for targeted drug delivery in TNBC. HMSN were synthesized *via* a modified Stober method and then loaded with Sa. The prepared nanoparticles were then characterized in terms of size, morphology, surface charge, and drug loading efficiency. *In vitro* release studies of the drug were conducted at pH 5.5 and 7.4 to mimic conditions of the tumor and normal physiological environment. The cytotoxicity of Sa@HMSN against MDA-MB-231 cells was also determined by MTT assay and the apoptotic cell death was analyzed through Ao/EtBr staining assay (Figure 1). The formation of salicylic acid-loaded hollow mesoporous silica nanoparticles (Sa@HMSN) as a targeted nanotherapeutic approach for triple-negative breast cancer is described in this work. Enhanced drug loading and pH-responsive release adapted to the acidic TNBC conditions are made possible by the special hollow-mesoporous design. Additionally, the study thoroughly assesses Sa@HMSN anticancer efficiency in MDA-MB-231 cells, demonstrating its capacity to perform over the drawbacks of traditional chemotherapeutic and nanoplatform strategies.

2. Results and discussion

2.1. Molecular docking analysis

Molecular docking simulations were performed to evaluate the binding affinity and interaction mechanism of salicylic acid (Sa) with the tumor suppressor protein p53 (PDB ID: 2OCJ), a critical regulatory protein in cell cycle arrest, DNA repair, and apoptosis, especially in the triple-negative breast cancer (TNBC) where p53 is often dysregulated. The study

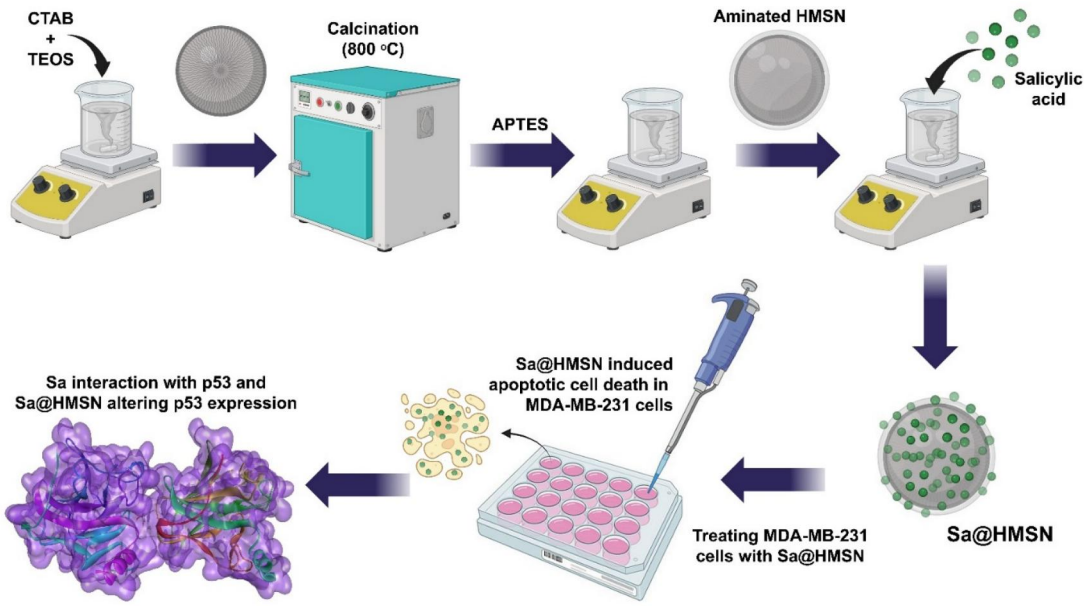

Figure 1. Schematic representation of the synthesis of salicylic acid-loaded hollow mesoporous silica nanoparticles (Sa@HMSN) and their p53-targeted anticancer activity in MDA-MB-231 breast cancer cells.

aimed to understand whether Sa, when delivered *via* HMSN, could engage in direct interaction with p53 to potentiate tumor-suppressive effects. Docking was performed using AutoDock Vina integrated within PyRx 0.8, and the resulting binding affinity was observed to be −5.5 kcal/mol, indicating moderate but biologically relevant binding strength. This energy value falls within a favorable range for small-molecule interactions with protein targets and supports the hypothesis that Sa can form a stable complex with p53.[20] The interaction analysis using BIOVIA Discovery Studio provided critical insights into the specific residues involved in stabilizing the Sa + p53 complex.

As shown in Figure 2, two key conventional hydrogen bonds were formed between the Sa and p53, as a donor with CYS275, while ASN239 as an acceptor with an observed bond length of 2.04 and 2.67 Å, indicating stronger and directionally favorable interactions essential for ligand retention and specificity. In addition to H-Bond interactions, hydrophobic π-alkyl contacts were identified with PRO152 and LEU137, with interatomic distances of 4.72 and 5.36 Å, respectively. These interactions enhance ligand stability by contributing to van der Waals and π-stacking interactions, which are commonly observed in drug-like compounds.[21] The current docking results provides strong mechanistic rationale for using Sa to enhance intracellular trafficking and p53 engagement in TNBC cells.

2.2. Structural morphology analysis

The morphological characteristics of the synthesized hollow mesoporous silica nanoparticles (HMSN) and salicylic acid-loaded HMSN (Sa@HMSN) were analyzed using scanning electron microscopy (SEM) and transmission electron microscopy (TEM) and the results are shown in Figure 3. The analysis aimed to observe changes in size, surface texture, and structural integrity following drug loading. As can be seen from Figure 3, bare HMSN exhibit a uniform spherical morphology with a relatively smooth surface. The particles appeared monodispersed with an average size distribution below 200 nm, which is ideal for passive tumor targeting *via* the enhanced permeability and retention (EPR) effect. The SEM micrographs at lower and higher magnifications confirmed that the particles are densely packed but non-aggregated, maintaining uniform size and shape. The TEM image of bare HMSN clearly showed the characteristic hollow mesoporous structure with a thin silica shell and dark center, consistent with classic Stober method derived HMSN.[22]

Upon loading with salicylic acid (Sa), surface changes were clearly visible in TEM. The Sa@HMSN retained their spherical shape; however, the surface appeared rougher and slightly less defined in the SEM images, indicating surface modification through Sa dispersion onto the outer mesoporous matrix. The corresponding TEM image of Sa@HMSN further support this observation. In addition, high-resolution TEM provided a closer appearance of the hollow mesoporous surface structure, which remained intact post-loading, confirming the structural robustness of the silica surface. The selected area electron diffraction (SAED) pattern showed a diffused ring, indicating the amorphous nature of the silica material, as expected for HMSN.[23] The structural conservancy of HMSN after drug loading, along with their morphological integrity, is crucial for efficient drug delivery. Maintaining the porous and hollow structure ensures high drug loading capacity and allows for controlled release in acidic environments (tumor microenvironment). Overall, the SEM and TEM results strongly confirm the successful synthesis of monodispersed spherical hollow silica nanospheres and their efficient loading ability. These nanostructures are structurally suited for targeted cancer therapy, combining favorable morphology, high surface area, and robust hollow mesoporous structure for drug delivery applications.

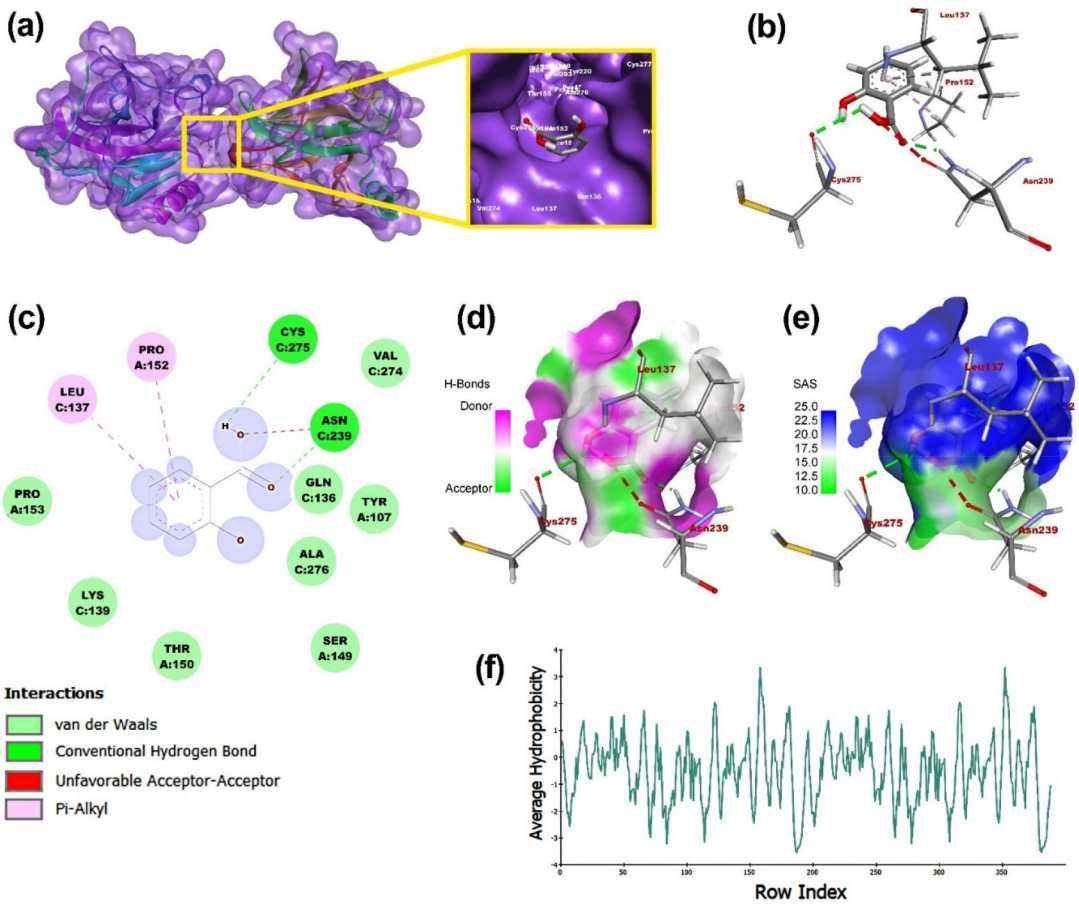

Figure 2. Molecular docking analysis of Sa with P53. (a) Surface structure of p53 showing the binding pocket occupied by Sa. (b) 3D Stick model depicting interactions between Sa and amino acid residues. (c) 2D interaction diagram showing conventional hydrogen bonding (green), π–alkyl interactions (pink), and Vander Waals forces. (d) H-Bond surface rendering showing donor (violet) and acceptor (green) fields. (e) Solvent accessible surface (SAS) visualization highlighting molecular compatibility. (f) Hydrophobicity plot of the p53 pocket region indicating favorable ligand site interactions.

2.3. Elemental analysis

The elemental composition and distribution of the synthesized HMSN and Sa-loaded HMSN (Sa@HMSN) were characterized using Energy Dispersive X-ray Spectroscopy (EDX) and elemental mapping, as shown in Figure 4. EDX spectra confirmed the presence of primary elements such as silicon (Si), oxygen (O), and carbon (C), which are expected components of silica-based nanocarriers and organic drugs. In the bare HMSN sample, two intense peaks corresponding to Si Kα and O Kα were observed with atomic percentage of 37.1 and 62.9%, verifying the silica framework composition. The presence of silicon and oxygen at strong intensities is consistent with the typical SiO_2 based network that forms the backbone of hollow mesoporous silica nanoparticles.[24] The Sa@HMSN showed an additional peak corresponding to C Kα (atomic percentage of 6.2%), which was absent in the bare HMSN. The presence of a distinct carbon peak indicates the successful incorporation of the organic drug Sa within the HMSN framework. The slight reduction in Si (atomic percentage of 30.1%) may result from surface coverage by the drug (Sa) molecules, which modulate the electron penetration depth during EDX analysis.

Elemental mapping further confirmed the uniform distribution of the elements. For bare HMSN, the signals of the elements Si and O were uniformly dispersed, consistent with a homogenous silica structure. Upon loading with Sa, the mapping of C in Sa@HMSN was found to be evenly distributed throughout the structure, suggesting internal entrapment and surface adsorption of the drug (Sa) molecules. The co-localization of Si, O, and C in Sa@HMSN confirms both the retention of the hollow mesoporous silica structure and the successful integration of the drug (Sa) molecules. Moreover, the preserved intensity of the Si and O peaks in Sa@HMSN confirms that the silica framework remains structurally stable post-loading. Overall, EDX and elemental mapping studies provide direct visual and quantitative evidence of the successful Sa incorporation into HMSN, confirming that the original silica framework remains intact.[7,25]

2.4. Particle size and stability analysis

Dynamic light scattering measurements revealed that the average particle side (diameter) of bare HMSN was 137 nm, whereas that of Sa@HMSN increased to 154 nm (Figure 5(a)), confirming successful drug loading. The increase in particle size is consistent with Sa molecules adsorbing onto the surface or occupying the mesopores, thereby increasing

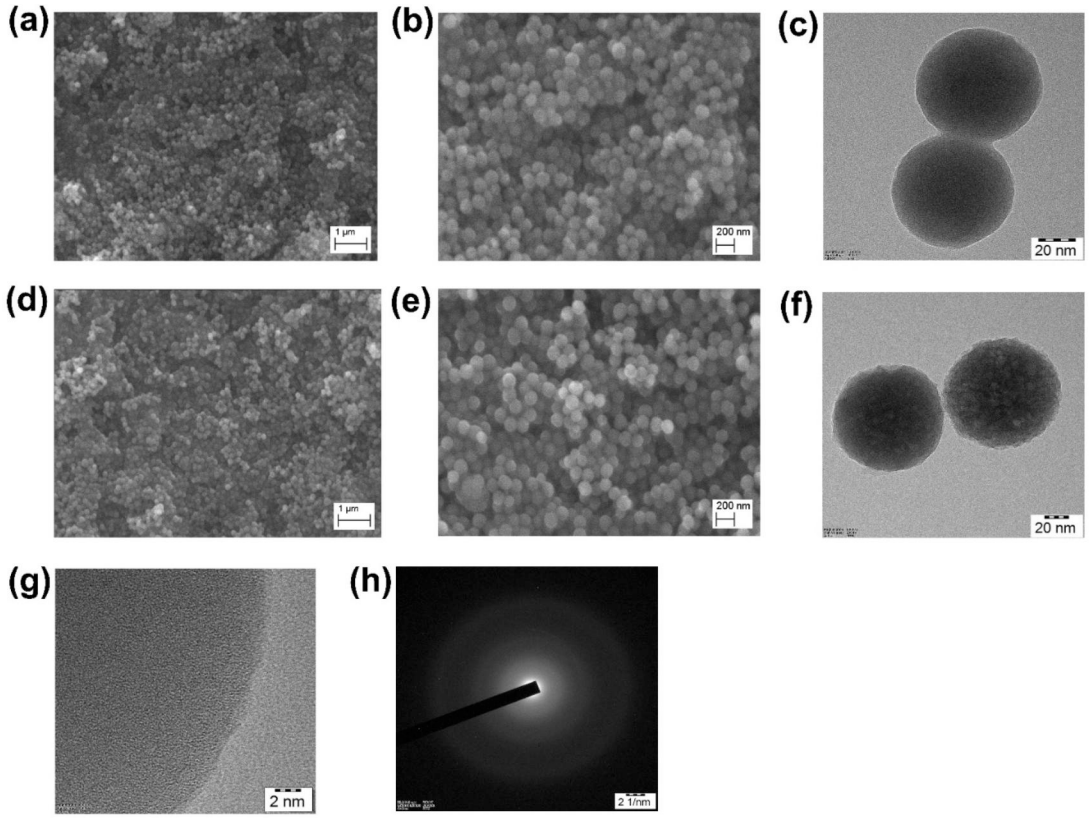

Figure 3. SEM and TEM images of HMSN and Sa@HMSN. (a–c) Bare HMSN, (a) SEM at 1 µm magnification, (b) SEM at 200 nm magnification, and (c) TEM showing uniform hollow structure at 20 nm magnification. (d–f) Sa@HMSN, (d) SEM at 1 µm magnification, (e) SEM at 200 nm magnification, and (f) TEM indicating roughened surface and internal density from Sa loading at 20 nm. (g) HR-TEM showing wall thickness and structural integrity at 2 nm. (h) SAED pattern confirming amorphous silica nature.

the overall diameter. Zeta potential measurements indicated that both samples exhibited negative surface charges, with HMSNs showing −31.4 mV and Sa@HMSN showing −38.7 mV (Figure 5(b)). The increase in negative surface potential after drug loading could be due to the deprotonation of acidic groups present in Sa and enhanced surface exposure of negatively charged species. A zeta potential below −30 mV generally signifies good colloidal stability in suspension, which is vital for drug delivery applications.[26]

2.5. XRD analysis

X-ray diffraction patterns of bare HMSN and Sa@HMSN were recorded in the 2θ range of 10 to 80° and the graphical representation of XRD is depicted in Figure 5(c). Bare HMSN displayed a broad diffraction peak centered around 22°, typical of amorphous silica. After Sa loading, the XRD pattern of Sa@HMSN retained this broad peak, indicating that the amorphous nature of the silica matrix remained intact. However, a slight increase in baseline intensity was observed in the Sa@HMSN pattern, which may be attributed to the dispersed Sa molecules within the pores or on the surface of HMSN. Very small sharp crystalline peaks of Sa were noted, indicating that the drug exists in a molecularly dispersed and amorphous state inside the silica framework. This form is beneficial for improving drug solubility and bioavailability. Such amorphous encapsulation has been reported to enhance the dissolution profile of hydrophobic drugs when delivered *via* mesoporous carriers.[27]

2.6. FTIR spectrum analysis

The FTIR spectra of both HMSN and Sa@HMSN were recorded in the range of 4000–400 cm^{-1} to identify the characteristic functional groups and the results are represented in Figure 5(d). For bare HMSN, the spectrum displayed a prominent absorption band around 1085 cm^{-1} corresponding to Si–O–Si asymmetric stretching, a band at 800 cm^{-1} for Si–O symmetric stretching, and a band near 460 cm^{-1} indicating Si–O bending vibrations. The broad band at 3420 cm^{-1} (approximately) represents O–H stretching, due to surface hydroxyl groups adsorbed on the silica's surface. Upon drug (Sa) loading, the FTIR spectrum of Sa@HMSN showed a shift and the appearance of additional peaks. A new band appeared at ∼1610 cm^{-1}, attributed to C = O stretching vibrations of carboxylic acid groups from Sa, and another at ∼1465 cm^{-1} corresponding to aromatic C = C stretching, confirming successful encapsulation of the salicylic acid. The reduced intensity of the hydroxyl stretch band indicates interaction between silanol (Si–O–H) groups of HMSN and hydroxyl or carboxyl groups of Sa, likely through hydrogen bonding or electrostatic interactions.[28] These spectral shifts and the appearance of specific bands for salicylic acid in the Sa@HMSN confirm that the drug

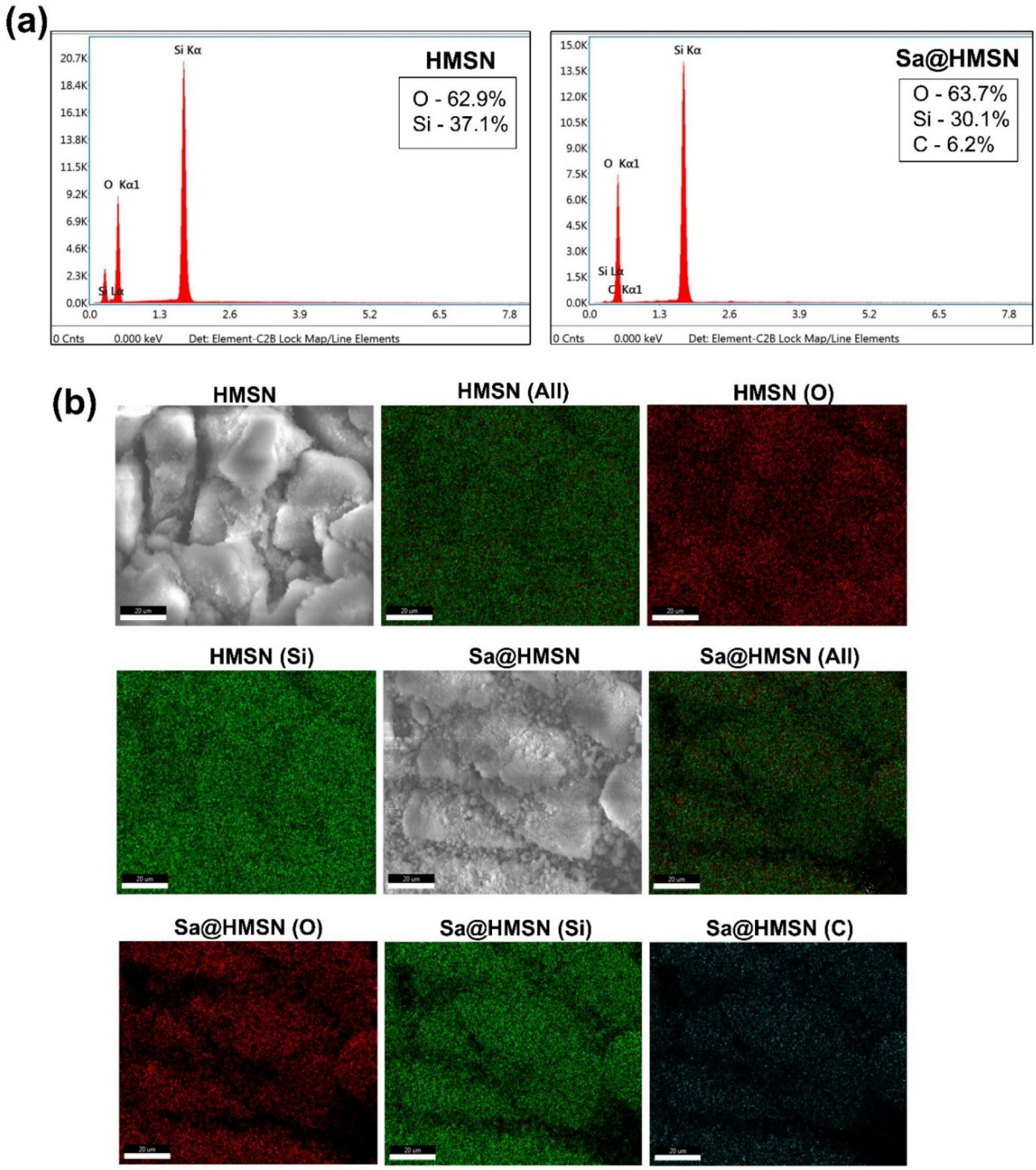

Figure 4. EDX and elemental mapping of HMSN and Sa@HMSN. (a) EDX spectrum of bare HMSNs showing peaks for Si and O and Sa@HMSN showing additional C peak indicating drug presence. (b) Elemental mapping images of bare HMSN and Sa@HMSN showing distribution of Si, O, and C with a magnification of 20 µm.

has been efficiently incorporated into hollow mesoporous silica nanostructure without disrupting its core assembly.

2.7. BET analysis

BET analysis was used to determine the pore volume, size, and surface area of bare HMSN and Sa@HMSN. The N_2 adsorption-desorption isotherm and pore size distribution of the bare HMSN and Sa-loaded HMSN are displayed in Figure 5(e). The mesoporous properties of bare HMSN, with a pore volume of 0.193 cc/g and a surface area of 64.59 m^2/g, were validated by BET analysis. Subsequent loading of salicylic acid, a reduction in surface area (28.14 m^2/g) and pore volume (0.158 cc/g) was observed, demonstrating that Sa molecules filled the hollow chambers and mesoporous channels, decreasing the available surface area for nitrogen adsorption. Isotherms have a type IV profile, which is characteristic of mesoporous materials, accordance to the IUPAC grouping. At minimal relative pressure ($P/P_0 < 0.1$), a gradual increase in adsorption volume was observed, demonstrating the presence of micropores that significantly boost surface area in the bare HMSN. In bare HMSN, there is a significant increase in the adsorption volume at elevated relative pressure ($P/P_0 > 0.8$) that is accounted for by

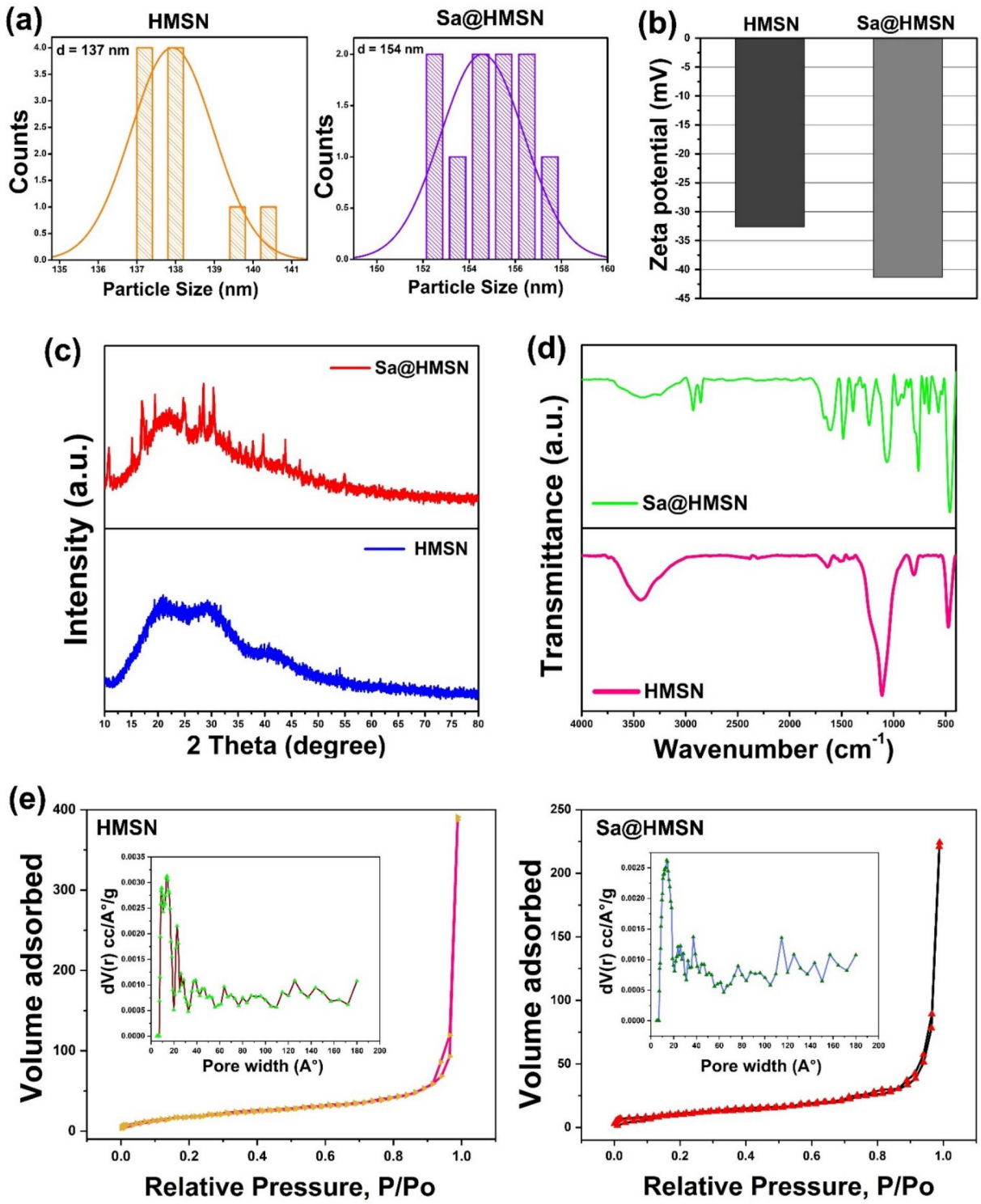

Figure 5. FTIR, XRD, particle size, zeta potential, and BET characterization of HMSN and Sa@HMSN. (a) Particle size distributions and (b) zeta potential analysis of HMSN and Sa@HMSN. (c) The XRD pattern of bare HMSN and Sa@HMSN. (d) FTIR spectra showing characteristic functional group changes post drug load. (e) Nitrogen adsorption-desorption isotherms and pore size distribution (inset figure) of HMSN and Sa@HMSN.

capillary condensation inside the mesopores. The emergence of a hysteresis loop at high relative pressures confirms the presence of interconnected mesoporous channels. The pore size distribution profile, which shows a broad pore size variation from microporous to mesoporous areas in the HMSN, confirms the formation of a hierarchical porous structure. A prominent peak in the 10 to 30 Å (1 to 3 nm) region indicates the presence of micropores and tiny mesopores in bare HMSN, which are primarily responsible for providing a wide surface area and an abundance of active sites. The Type IV behavior of the N_2 adsorption-desorption isotherm validates the mesoporous structure of the Sa-loaded HMSN. While capillary condensation in mesopores causes the abrupt increase in adsorption at relatively high pressure (*P*/

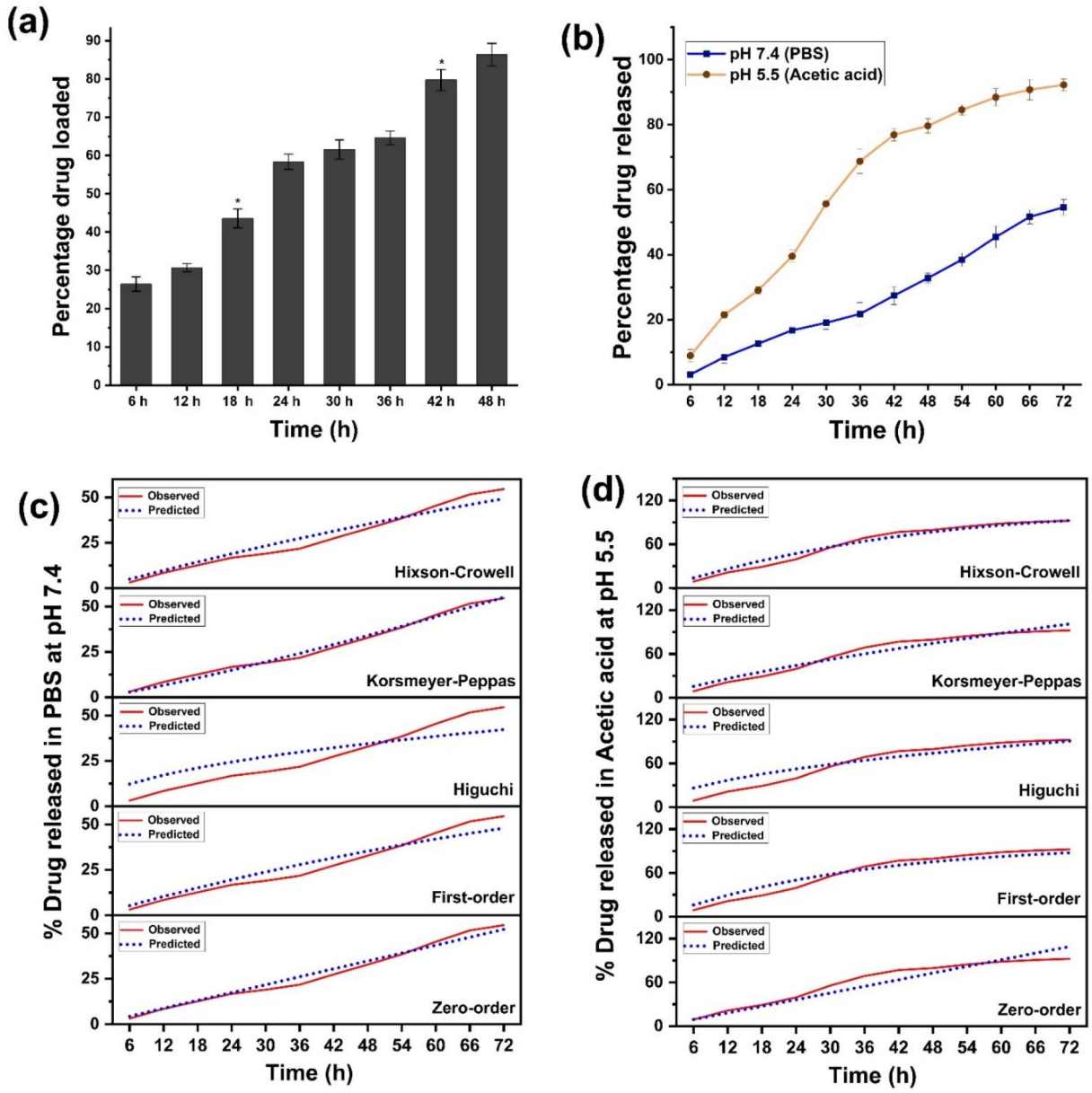

Figure 6. Drug load and release kinetics of Sa@HMSN. (a) Drug loading percentage over 48 h time. (b) *In vitro* Sa release at neutral pH 7.4 (PBS) and acidic pH 5.5 (acetic acid). Kinetic model fitting of Sa release profiles in five different models (observed and predicted) at two different pH conditions and solvents. (c) Neutral pH 7.4 (PBS) and (d) acidic pH 5.5 (acetic acid).

$P_0 > 0.8$), micropores are identified by a progressive nitrogen absorption at low relative pressure ($P/P_2 < 0.1$). The pore size distribution of Sa@HMSN, which displays both a broader spread and dominant pores in the 10 to 30 Å range, confirms a hierarchical micro-mesoporous structure.

2.8. Evaluation of drug load and release

The drug loading study was conducted over a 48-h period to evaluate the encapsulation capacity of HMSNs for Sa. As shown in Figure 6(a), the percentage of drug loaded increased progressively with time, confirming effective passive adsorption of Sa into the hollow mesoporous silica framework. At 6 h, the loading efficiency was ~26.4%, which increased steadily to 30.7% at 12 h, 43.5% at 18 h, and 58.4% at 24 h. The trend continued with 61.6% at 30 h, 64.6% at 36 h, and 79.74% at 42 h, ultimately reaching a maximum of 86.4% at 48 h. The consistent rise in loading percentage is attributed to the prolonged exposure of Sa to the high surface area and pore volume of HMSN, allowing more drug molecules to diffuse and interact with internal and external adsorption sites. After 42 h, the loading curve began to plateau, indicating saturation of available pores and surface binding sites. This behavior is typical for hollow mesoporous drug carriers where the rate of adsorption is initially rapid but slows down as the internal cavity fills up.[29]

To mimic physiological and tumor-specific environments, *in vitro* drug release studies were carried out in phosphate-buffered saline (PBS, pH 7.4) and acetic acid buffer (pH 5.5) over a period of 72 h. As illustrated in Figure 6(b), the release kinetics of salicylic acid (Sa) from HMSNs were strongly dependent on the pH of the release medium.

Under acidic conditions (pH 5.5), Sa exhibited a significantly faster and higher cumulative release compared to physiological pH (7.4). Within the initial 6 h, 8.92% of Sa was released at pH 5.5, whereas only 3.12% was released in PBS. After 24 h, the cumulative release increased to 39.51% in acetic acid, in contrast to 16.74% at pH 7.4. This difference became more pronounced over time, with 88.42% release observed at 60 h and a maximum of 92.24% at 72 h under acidic conditions, while only 54.57% release was achieved at pH 7.4. A noticeable acceleration in drug release was observed between 24 and 42 h at pH 5.5, indicating a pH-responsive release profile. This behavior can be attributed to partial degradation of the silica framework and reduced electrostatic interactions between Sa and the mesoporous silica matrix under acidic conditions. Hollow mesoporous silica nanoparticles (HMSN) are essential for improving salicylic acid's apparent solubility and dissolving behavior, in addition to facilitating pH-responsive release. Small-molecule medications like salicylic acid have poor water solubility, that can impair their bioavailability and therapeutic efficiency. In the current work Sa is encapsulated in the mesoporous structure of HMSN, which increases the drug's dissolution rate by changing it from a crystalline state to a partly amorphous form. The large surface area and confined nanoscale pores of HMSN significantly rise the effective drug-solvent interfacial part, facilitating rapid wetting and diffusion of the Sa molecules into the surrounding medium. Such pH-triggered release is highly desirable for cancer therapy, as it enables preferential drug release in the acidic tumor microenvironment while minimizing premature drug leakage under normal physiological conditions.[30]

2.9. Release kinetics profile

To determine the mechanism governing Sa release from HMSN, the experimental data were fitted to five kinetic models: Zero-order, First-order, Higuchi, Korsmeyer-Peppas, and Hixson-Crowell, and the model fitness was evaluated at both pH 5.5 (acetic acid) and 7.4 (PBS) as depicted in Figure 6(c) and Table 1. Under physiological (pH 7.4, PBS) and acidic (pH 5.5, acetic acid) conditions, the *in vitro* release of salicylic acid (Sa) from hollow mesoporous silicon nanoparticles (HMSN) demonstrated distinct pH-dependent behavior. The Korsmeyer-Peppas and Zero-order models demonstrated the best match ($r^2 = 0.99$), indicating a diffusion-relaxation linked process with nearly constant release. At pH 7.4, Sa release was comparatively sustained and regulated. On the other hand, a significantly greater release rate constant was found at pH 5.5 in acetic acid, indicating faster drug diffusion as a result of protonation effects and partial silica framework dissolution. Acidic release was well characterized by the First-order and Hixon-Crowell models, which supported concentration-dependent release with kinetics aided by erosion. The release mechanism in the current work was non-Fickian (anomalous transport) at both pH 7.4 and pH 5.5, as demonstrated by the Korsmeyer-Peppas release exponent ($n > 0.5$). Overall, the kinetic study shows that HMSN provide regulated, pH-responsive Sa release, thereby facilitating quick drug availability in acidic environments that are relevant to tumor microenvironments.[31]

2.10. Cytotoxic evaluation

The cytotoxic effect of HMSN, Sa, and Sa@HMSN was evaluated on MDA-MB-231 breast cancer cells using the MTT assay. Cell viability was assessed after 24 h of treatment at increasing concentrations ranging from 5 to 35 µg/mL. Additionally, the morphological alterations associated with cell damage post treatment was observed and compared with untreated cells and the results are presented in Figure 7. The bare HMSN exhibited negligible cytotoxicity across all tested concentrations and the cell viability remained above 92% even at the highest dose of 35 µg/mL, confirming the excellent biocompatibility and less-toxic nature of the hollow mesoporous silica nanocarrier. Free salicylic acid (Sa) displayed a clear dose-dependent cytotoxic effect and the cell viability declined from 87.26% at 5 µg/mL to 81.55% at 10 µg/mL, 70.09% at 15 µg/mL, 58.29% at 20 µg/mL, and 37.69% at 35 µg/mL, demonstrating its anticancer potential in a dose-

Table 1. Calculated drug release kinetics models for Sa@HMSN.

		Sa@HMSN	
Model	Parameter	pH 7.4 (PBS)	pH 5.5 (acetic acid)
Zero order $F = K_0 \times t$	K_0	0.725	1.516
	r^2	0.992	0.903
	AIC	52.219	84.083
First order $F = 100 \times [1 - \text{Exp}\ (-K_1 \times t)]$	K_1	0.009	0.029
	r^2	0.935	0.942
	AIC	65.923	77.941
Higuchi model $F = \text{KH} \times t_{1/2}$	kH	4.977	10.697
	r^2	0.756	0.878
	AIC	81.882	86.819
Korsmeyer-Peppas model $F = \text{kKP} \times t^n$	kKP	0.347	4.059
	r^2	0.992	0.954
	n	1.184	0.752
	AIC	43.465	77.027
Hixon-Crowell model $F = 100 \times [1 - (1 - {}_k\text{HC} \times t)^3]$	kHC	0.003	0.008
	r^2	0.952	0.973
	AIC	62.379	68.610

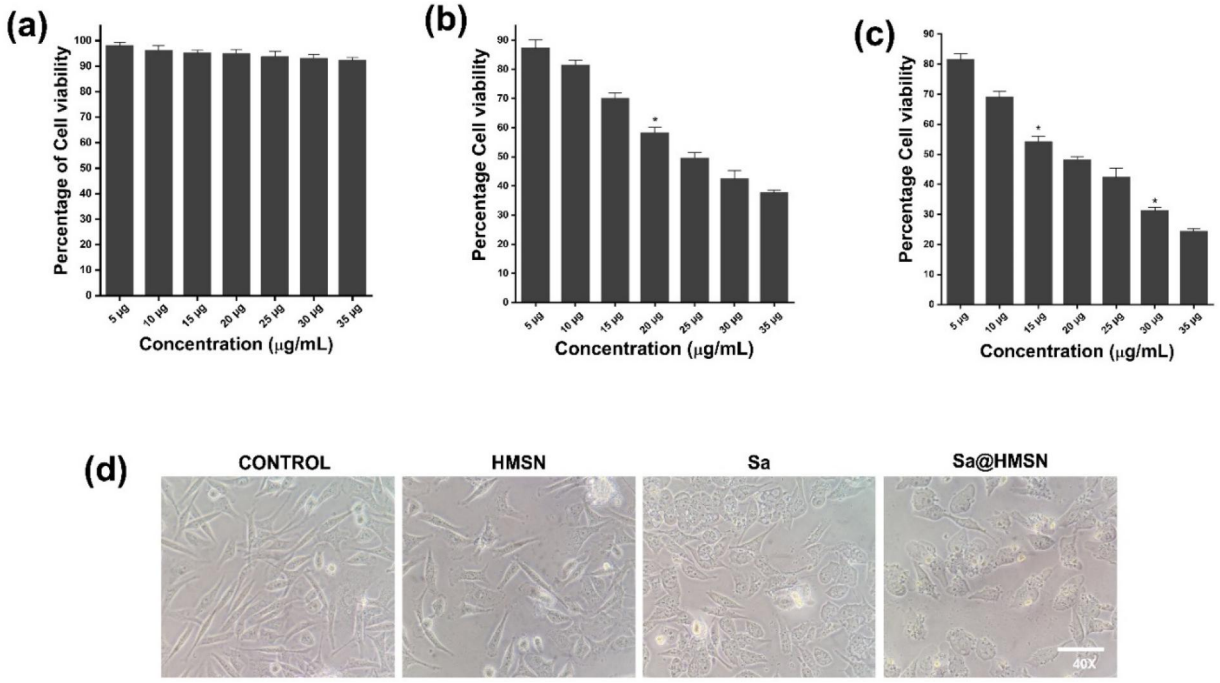

Figure 7. Cytotoxicity of HMSN, Sa, and Sa@HMSN in MDA-MB-231 cells. MTT assay results showed minimal cytotoxic effects in (a) bare HMSN and dose-dependent decrease in cell viability when treated (b) free Sa and (c) Sa@HMSN. (d) microscopy images showing morphology of control, HMSN, Sa, and Sa@HMSN treated cells using 40 × objective lens.

dependent manner. The formulated Sa@HMSN treatment showed enhanced cytotoxicity compared to free salicylic acid. In the dosage of 5 μg/mL viability was 81.60%, decreasing further to 69.03% at 10 μg/mL, 54.29% at 15 μg/mL, 48.27% at 20 μg/mL, and approaching 24.39% at 35 μg/mL. The IC_{50} dosage of bare Sa was calculated to be 24.97 μg/mL and the Sa-loaded HMSN exhibited an IC_{50} dosage of 17.01 μg/mL. The enhanced cytotoxicity is attributed to targeted release of Sa through nanoparticle-mediated delivery within the MDA-MB-231 cells. The microscopic form was investigated, and the control cells exhibited normal elongated fibroblastic morphology, whereas HMSN treated cells showed no morphological changes, supporting its biocompatibility. The free Sa treated cells exhibited early apoptotic signs such as cell rounding, shrinkage, and detachment and the formulated Sa@HMSN treated cells showed noticeable apoptotic topographies such as cell rounding, reduced adhesion, and increased cell debris, indicating enhanced intracellular drug accumulation and apoptotic induction *via* the nanoparticle delivery route.[32]

2.11. Apoptosis evaluation through Ao/EtBr dual staining

The apoptotic potential of salicylic acid loaded hollow mesoporous silica nanoparticles (Sa@HMSN) in MDA-MB-231 breast cancer cells was assessed using acridine orange/ethidium bromide (Ao/EtBr) dual fluorescent staining for 24 h. As shown in Figure 8(a), living cells emitted green fluorescence, early apoptotic cells showed yellowish-green nuclei, late apoptotic and necrotic cells fluoresced orange and red. Quantitative analysis (Figure 8(b)) revealed that control cells displayed minimal apoptosis, with early apoptotic rate of 1.0%.

Cells treated with blank HMSN exhibited cell death percentage of 2% as early apoptosis, 1% as late apoptosis, confirming the negligible cytotoxicity of the nanocarrier itself. Treatment with free salicylic acid significantly increased apoptotic cell death, showing 24% of early apoptosis and 17% of late apoptosis, along with 7% of necrotic cells and the Sa@HMSN treated cells exhibited the maximum level of cell death, with 19% early apoptosis and 31% late apoptosis. Necrotic death also increased to 11%, indicating effective cellular disruption at prolonged exposure. The enhanced apoptosis observed in the Sa@HMSN group is attributed to improved intracellular delivery and sustained release of salicylic acid, which likely maintains therapeutic intracellular concentrations over a longer period. These findings confirm that hollow mesoporous silica nanocarrier demonstrated superior apoptotic induction through sustained release and improved cellular uptake of Sa in breast cancer cells.[33]

2.12. Immunocytochemistry analysis

To further investigate the functional modification induced by salicylic acid loaded HMSN (Sa@HMSN) immunocytochemistry (ICC) was performed and the expression level of tumor suppressor protein p53 post treatment was analyzed and is shown in Figure 8(c). The intensity of the p53 expression analysis is shown in Figure 8(d). The analysis was conducted using the horseradish peroxidase (HRP) conjugated detection

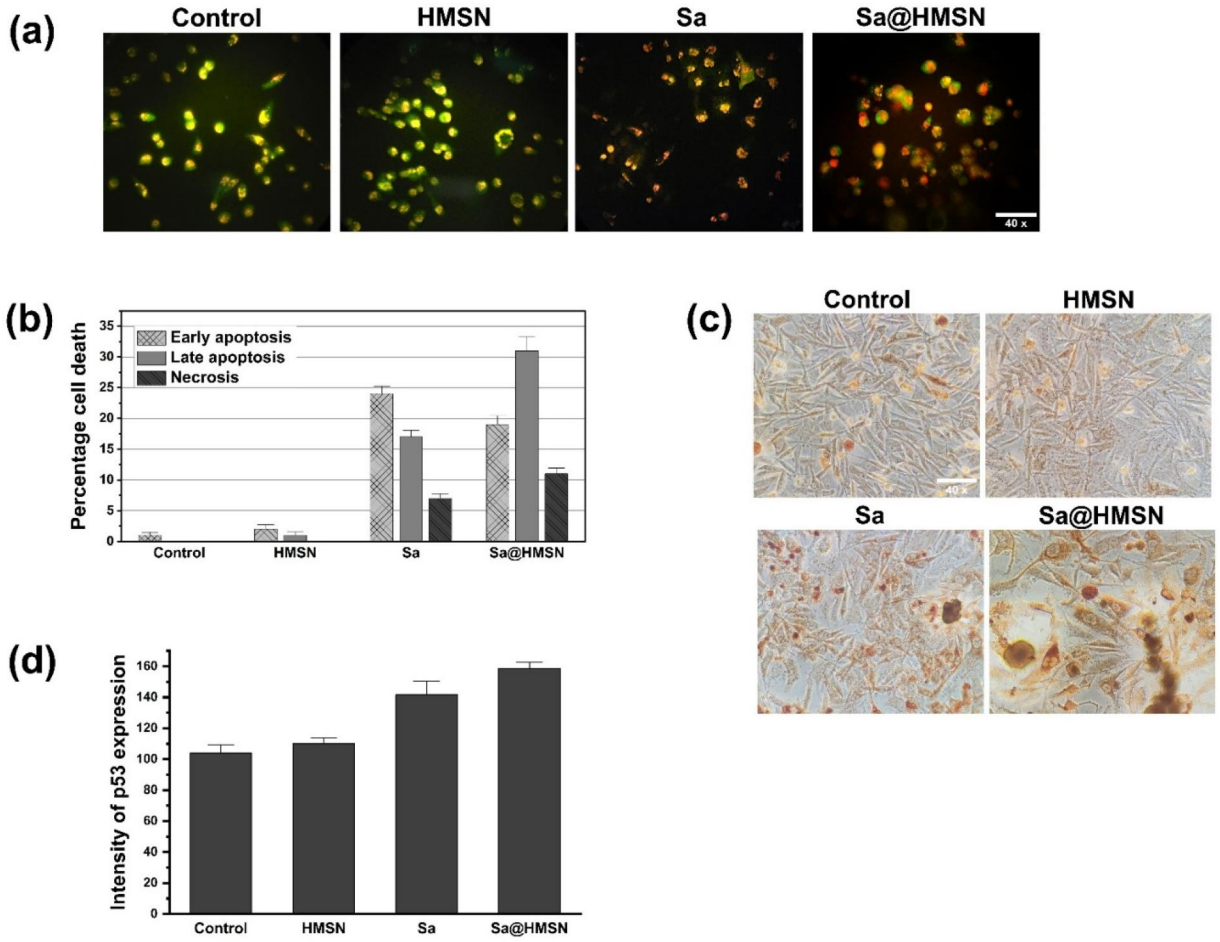

Figure 8. Apoptosis analysis of MDA-MB-231 cells treated with Sa@HMSN using AO/EtBr staining. (a) Fluorescence images show cells after 24 h treatment with Control, HMSN, Sa, and Sa@HMSN. (b) Bar graph shows percentage of cell death under different stages of apoptosis. (c) Immunocytochemistry images showing p53 expression (brown staining) in Control, HMSN, Sa, and Sa@HMSN-treated cells. The free Sa and Sa@HMSN groups show more intense brown staining, indicating higher p53 expression. (d) Bar graph representing the intensity of p53 expression. Sa@HMSN-treated cells show the highest p53 expression, followed by free Sa, while HMSN and Control show comparatively lower expression levels.

method, with diaminobenzidine (DAB) and the chromogen, resulting in brown nuclear staining indicative of p53 localization. In the control group, basal p53 expression was observed with an average intensity of ~103.89 and HMSN treated groups exhibited a comparable expression level of 110.04, confirming the non-intrusive nature of the HMSN material on p53 regulation. The treatment with free Sa has shown significant elevation of p53 expression to around 141.62, indicative of DNA damage and cellular stress induced activation. Notably, cells treated with Sa@HMSN exhibited greater intensity of p53 expression with 158.57, exhibiting a more robust activation of p53 dependent apoptotic signaling. Microscopic observations support the quantitative data, a marked increase in the number of brown-stained nuclei was observed in the Sa and Sa@HMSN groups with intense and widespread nuclear staining. The elevated p53 expression post treatment of Sa@HMSN shows that the nanocarrier significantly enhances the bioavailability and intracellular retention of Sa, which in turn promotes p53-mediated apoptosis.[34] These findings confirm that the Sa@HMSN formulation not only improves delivery efficiency but also amplifies tumor suppressor responses, further confirming its therapeutic potential in triple-negative breast cancer treatment.

3. Materials and methods

3.1. Molecular docking studies

The molecular docking experiment was performed with the PyRx 0.8 virtual screening software created by The Scripps Research Institute, San Diego, USA, to examine the binding affinity of salicylic acid (Sa) to the P53 protein, an important controller in breast cancer signaling cascades. The 3D coordinate of the target protein P53 (PDB ID: 2OCJ) was downloaded from the RCSB Protein Data Bank (https://www.rcsb.org), and the structure of the ligand Sa was downloaded from the PubChem database (CID: 338) (https://pubchem.ncbi.nlm.nih.gov). The protein was pre-processed before docking by deleting water molecules, adding polar hydrogens, and imposing Kollman charges using AutoDock Tools. The ligand Sa was minimized in energy and transformed to the desired format. The docking process was performed with AutoDock Vina, which is embedded in PyRx, to model the interaction of Sa with P53's active site. Following docking, the most

scored conformation with the minimum binding energy was chosen for subsequent studies. The profiles of interaction, such as hydrogen bonding and hydrophobic contacts, were visualized through BIOVIA Discovery Studio Visualizer to determine the residues of binding that are responsible for stabilizing the Sa + P53 complex.

3.2. Chemicals and reagents

Tetraethyl orthosilicate (TEOS), cetyltrimethylammonium bromide (CTAB), ammonia solution, ethanol, salicylic acid (SA), and all other chemicals were of analytical grade and purchased from Sigma-Aldrich (St. Louis, MO, USA). Dimethyl sulfoxide (99.7%), phosphate buffered saline (cell culture grade), thiazolyl blue tetrazolium bromide (≥97.5%), acridine orange (≥98%), and ethidium bromide (∼95%, HPLC grade) were purchased from Sigma-Aldrich, India. Invitrogen, Carlsbad, CA, USA; provided Dulbecco's modified eagle medium (DMEM), 0.25% trypsin EDTA (Gibco), and fetal bovine serum (FBS). 18 MW milli-Q water 133 (Millipore system, Burlington, MA, USA) was used to generate all of the test solutions. Reagents and other chemicals of analytical quality were acquired from Thermo Fisher Scientific Ltd. in Mumbai, India. The PolyExcel HRP/DAB detection system and the primary antibody p53 used in this investigation were acquired from PathnSitu Biotechnologies in Hyderabad, India. PolyExcel peroxidase block, PolyExcel target binder, PolyExcel poly HRP, PolyExcel stunn DAB buffer, PolyExcel stun DAB chromogen, and immuno wash buffer are the components of the detection system. The remaining chemicals were purchased from Sigma Aldrich in India, including phosphate buffered saline with 0.05% tween 20, hematoxylin (Harris solution), and paraformaldehyde powder (95% purity). The human triple-negative breast cancer cell line MDA-MB-231 was obtained from the National Center for Cell Science (NCCS), Pune, India.

3.3. Synthesis of HMSN

Hollow mesoporous silica nanoparticles (HMSN) were synthesized using a modified Stober method.[35] A white precipitate was typically achieved by dissolving 0.08 g of CTAB and 500 μL of TEOS at 300 rpm, then adding 500 μL of a 25% ammonia solution in 40.50 mL of an ethanol and double distilled water as solvent and stirring the mixture at 700 rpm for 3 h at 30 °C. CTAB acts as a structure-directing surfactant, forming micellar templates that govern mesoporous architecture and pore size of hollow mesoporous silica nanoparticles. TEOS performs as silica precursor, undergoing hydrolysis and condensation to form a uniform mesoporous silica shell with a hollow interior. Subsequent removal of CTAB causes the formation of the mesoporous structure essential for high drug loading and controlled release. The quantities of CTAB and TEOS used in this synthesis process were selected and optimized based on established protocols reported in previous literature.[36] Centrifugation at 8000 rpm for 8 min produced the final product, which was then washed with 100% ethanol and double distilled water before being allowed to air dry. At 800 °C, the dried product was calcined for 8 h. After calcination, 100 mL of 100% ethanol, 100 mg of HMSN, and 100 μL of APTES were combined, and the mixture was allowed to stir at room temperature for an entire day. After centrifugation for 24 h, amine-functionalized HMSN was produced, and it was washed with ethanol and double-distilled water.

3.4. Drug loading and release studies

To load salicylic acid (Sa) into HMSN, 100 mg of HMSNs were dispersed in 100 mL of ethanol containing 100 of Sa. The mixture was stirred for 24 h at room temperature. The suspension was then centrifuged, and the Sa-loaded HMSN (SA@HMSN) was washed with double distilled water to remove any surface adsorbed drug particles and air dried. The amount of Sa loaded was determined by UV-Visible spectrophotometry at 297 nm using a calibration curve. The loading capacity of Sa@HMSN was determined by applying the formula, Percentage drug load = (OD at 0th hour − OD at 48th hour/OD at 0th hour) × 100. To evaluate the release profile, 10 mg of Sa@HMSN were suspended in 50 mL of phosphate-buffered saline (PBS) at 7.4 and acetic acid with pH 5.5, physiological conditions and simulating tumor, respectively.[37] The mixture was placed in a shaker incubator at 37 °C. At regular intervals 5 mL were taken out and replaced with new PBS (0, 6, 12, 18, 24, 30, 36, 42, 48, 54, 60, 66, and 72 h) in order to maintain sink conditions. The amount of Sa that was released was measured at 297 nm using UV-Visible spectrophotometry.

3.5. Drug release kinetics

To understand the release mechanism, data were fitted to five kinetic models: zero-order, first-order, Higuchi, Korsmeyer-Peppas, and Hixson-Crowell, using DDSolver, an Excel add-in for model-fitting.[38] The best-fitting model was selected based on regression coefficient (R^2) values. The kinetic modeling was performed using the DD Solver 1.0 add-in for Microsoft Excel, based on the experimentally obtained release profiles. Zero-order kinetics describes a constant drug release rate independent of concentration, whereas first-order kinetics assumes that the release rate is proportional to the remaining drug concentration. The Higuchi model interprets drug release as a diffusion-driven process, proportional to the square root of time, typically from an insoluble matrix. The Korsmeyer-Peppas model provides a semi-empirical relationship to characterize drug release behavior from polymeric systems. Finally, the Hixson-Crowell model provides additional understanding of the erosion-based mechanism of drug release by taking into consideration variations in surface area and particle size during the release process.[39]

3.6. Characterization of HMSN and Sa@HMSN

The morphology and structural features of the synthesized nanoparticles were characterized *via* scanning electron microscopy (SEM) using an Evo18 Zeiss instrument, Munich, Germany. Energy-dispersive X-ray spectroscopy (EDX) was performed in conjunction with SEM, revealing the elemental mapping and verifying the presence of silica and salicylic acid-associated elements with percentage. The cross-sectional surface texture and the presence of the characteristic hollow core structure of HMSN was assessed *via* Hi-Resolution Transmission electron microscopy (HR-TEM) using JEOL Japan, JEM-2100 Plus instrument. Fourier-transform infrared spectroscopy (FTIR) was applied to confirm the successful loading of salicylic acid (Sa) into the HMSN based on functional group assessment using Shimadzu IR Tracer-100 spectrometer (Kyoto, Japan). The samples were grinded well with the KBr pellet and the wavenumber were recorded with the range of 4000 to 400 cm^{-1}, respectively. X-Ray Diffraction (XRD) was performed to assess the nature of the nanomaterial by using Bruker D8 advance ECO XRD system (Karlsruhe, Germany) with an SSD160 1D Detector X-ray diffractometer. The samples were measured in the 2Θ range of 10 to 80°. The particle size of unloaded and drug-loaded nanoparticles and zeta potential of the HMSN and Sa@HMSN was determined using Nanoparticle Analyzer SZ-100 (Horiba, Kyoto, Japan) with temperature of the holder of 25.0 °C, dispersion medium viscosity of 0.894 mPa·s, conductivity of 0.079 mS/cm, and electrode voltage of 3.8 V. The particular surface area was determined employing the Brunauer Emmett Teller (BET) technique, and the pore size distribution and average pore volume were computed using the Barrett Joyner Halenda (BJH) system utilizing an Autosorb iQ-Chemisorption gas sorption analyzer. Together, these techniques confirmed the successful formation of HMSN, drug loading, and physiochemical stability.

3.7. Cytotoxicity assessment using MTT assay

The cytotoxic effect of Sa@HMSN was evaluated in MDA-MB-231 cells using the MTT assay.[40] Cells were cultured in DMEM containing 10% FBS and 1% penicillin-streptomycin under 5% CO_2 at 37 °C. Once 80% confluent, cells were trypsinized, counted, and seeded in 96-well plates. After 24 h, cells were treated with various concentrations of Sa@HMSN (5 to 35 µg/mL) for another 24 h. Following treatment, 10 µL of MTT solution was added to each well and incubated for 3 h under dark condition. The resulting formazan crystals were dissolved in 100 µL of DMSO, and absorbance was measured at 595 nm using a microplate reader. The percentage of viable cells was calculated relative to untreated controls. All experiments were performed in triplicate. The IC_{50} value of Sa@HMSN was used in further apoptosis and molecular evaluations. Percentage cell viability = (abs. of treated cells/abs. of untreated cells) × 100.

3.8. Apoptosis evaluation

To assess apoptosis induction by Sa@HMSN, MDA-MB-231 cells were seeded and treated with the IC_{50} concentration of Sa@HMSN for 24 h. After incubation, the cells were washed twice with PBS and stained with an acridine orange/ethidium bromide (Ao/EtBr) mixture for 15 min in the dark.[41,42] The stained cells were immediately examined under a fluorescence microscope (TCM-400, Labomed) using B-excitation and G-excitation filters. Morphological changes were analyzed to differentiate viable and apoptotic cells. Viable cells emitted green fluorescence with intact nuclei, while early and late apoptotic cells displayed orange to red fluorescence due to compromised membrane integrity and EtBr uptake.

3.9. Immunocytochemistry

For immunocytochemical detection of apoptosis-related proteins, Sa@HMSN-treated cells were fixed with 4% paraformaldehyde. After fixing the cells were washed twice with PBST each 5 min, followed by addition of peroxidase quencher in the fixed cells and then incubation for 10 min. Following incubation, cells were washed with immuno wash buffer for 5 min. After washing, the cells were treated with primary antibody anti-p53 for 1 h at room temperature in a moist atmosphere. The cells were washed with antibody wash buffer for 10 min and then treated with PolyExcel target binder. Following incubation, PolyExcel, PolyHRP was added for 10 min. The cells were then treated with DAB solution in the dark and incubated for 7 min after cleaned with immuno wash buffer. The cells were then examined under an inverted phase contrast microscope after receiving a mild hematoxylin counterstain. Using Image J software, the proteins' expression was measured and their intensity was computed.

3.10. Statistical analysis

Every experiment had three repetitions and was carried out in triplicate. The mean ± standard error was used to express the accuracy of the data. With a total number (n) of three, a one-way ANOVA statistical analysis was carried out to evaluate the outcomes between the control and all treatment samples (p-value < 0.05 represents significance, denoted by *).

4. Conclusion

In this study, we successfully developed and characterized a novel Sa@HMSN formulation for targeted triple-negative breast cancer therapy. The loading of salicylic acid into HMSN significantly improved its bioavailability and anticancer efficacy compared to free Sa. Molecular docking studies initially confirmed a stable interaction between Sa and the target protein p53, demonstrating its potential anticancer mechanism at the molecular level. The SEM and TEM analyses showed monodispersed spherical assembly of

the synthesized nanocarriers and the presence of Sa on the surface of HMSN. The amorphous nature of HMSN and Sa@HMSN was confirmed through XRD and the presence of functional groups of bare HMSN and Sa incorporated HMSN was confirmed *via* FTIR vibrational analysis. The particles were eventually dispersed and the element distribution associated with synthesized bare HMSN and the Sa-loaded HMSN was investigated through elemental mapping. The decrease in the Si peak intensity and the appearance of C peak in the EDX spectra confirmed the presence of Sa on the surface of HMSN. The drug load analysis showed that Sa was effectively incorporated in the pores and also on the surface of HMSN and the release profile exhibited a targeted and sustained release of salicylic acid from HMSN in the acidic environment (acetic acid pH 5.5). The *in vitro* cytotoxicity using the MTT assay revealed a significant reduction in cell viability in Sa@HMSN treated MDA-MB-231 cells, with an IC_{50} value of 17.01 µg/mL, which is lower than that of free Sa. This enhanced cytotoxic effect may be attributed to the controlled and sustained release of Sa from the hollow mesoporous silica structure. Further confirmation through Ao/EtBr dual staining demonstrated that Sa@HMSN induced significantly higher levels of apoptosis (early and late stages) compared to free Sa, HMSN, and control. Immunocytochemical analysis of p53 expression revealed a significant expression of p53 in Sa@HMSN treated cells, which aligns with the increased apoptotic activity. As p53 plays a crucial role in cell cycle arrest and apoptosis, its upregulation indicates that Sa@HMSN mediates tumor suppression *via* a p53-dependent pathway. Taken together, the results of this study strongly indicate that Sa@HMSN is a promising nanoformulation capable of enhancing the anticancer efficacy of salicylic acid through targeted delivery, sustained release, and activation of apoptosis *via* the p53 pathway. Despite promising *in vitro* findings, the present study lacks *ex vivo* or *in vivo* evaluations. Future investigations incorporating hemocompatibility, serum stability, and *in vivo* systemic toxicity assessments are essential to validate the biosafety profile of Sa@HMSN.

Acknowledgments

The authors are grateful to the Biomaz Infosearch, Madurai, Tamil Nadu, India for the technical support and research facilities. .

Ethical approval

This article does not contain any studies with human or animal subjects performed by any of the authors.

Author contributions

CRediT: **Sureba Sukumaran**: Conceptualization, Data curation, Formal analysis, Investigation, Methodology, Software, Validation, Visualization, Writing – original draft, Writing – review & editing; **Jyothi Kanagaraj**: Data curation, Formal analysis, Investigation, Methodology, Project administration, Resources, Validation, Visualization, Writing – review & editing; **Mohana Priya**: Formal analysis, Methodology, Resources, Validation, Writing – original draft; **Priya Rajan**: Investigation, Software, Validation, Writing – review & editing; **Azar Zochedh**: Conceptualization, Data curation, Formal analysis, Investigation, Methodology, Project administration, Resources, Software, Supervision, Validation, Visualization, Writing – original draft, Writing – review & editing.

Disclosure statement

No potential conflict of interest was reported by the author(s).

Funding

No external funding was provided for this work.

ORCID

Sureba Sukumaran http://orcid.org/0000-0003-0780-9577
Jyothi Kanagaraj http://orcid.org/0009-0009-2239-2459
Mohana Priya http://orcid.org/0000-0002-9627-4721
Azar Zochedh http://orcid.org/0000-0001-9818-5071

Data availability statement

Data sharing not applicable to this article as no datasets were generated or analyzed during the current study.

Usage of artificial intelligence

The online tool QuillBot, an AI-powered writing assistant, was used to check grammatical accuracy and language clarity in this manuscript. No AI-generated content was used in the conceptualization, analysis, or interpretation of the study results.

References

[1] Hassanpour, S. H.; Dehghani, M. Review of Cancer from Perspective of Molecular. *J. Cancer Res. Pract.* **2017**, *4*, 127–129. DOI: 10.1016/j.jcrpr.2017.07.001.
[2] Giaquinto, A. N.; Sung, H.; Miller, K. D.; Kramer, J. L.; Newman, L. A.; Minihan, A.; Jemal, A.; Siegel, R. L. Breast Cancer Statistics, 2022. *CA Cancer J. Clin.* **2022**, *72*, 524–541. DOI: 10.3322/caac.21754.
[3] Kumar, P.; Aggarwal, R. An Overview of Triple-Negative Breast Cancer. *Arch. Gynecol. Obstet.* **2016**, *293*, 247–269. DOI: 10.1007/s00404-015-3859-y.
[4] Xu, L.; Xu, P.; Wang, J.; Ji, H.; Zhang, L.; Tang, Z. Advancements in Clinical Research and Emerging Therapies for Triple-Negative Breast Cancer Treatment. *Eur. J. Pharmacol.* **2025**, *988*, 177202. DOI: 10.1016/j.ejphar.2024.177202.
[5] Tezcan, O.; Elshafei, A. S.; Benderski, K.; Rama, E.; Wagner, M.; Moeckel, D.; Pola, R.; Pechar, M.; Etrych, T.; von Stillfried, S.; et al. Effect of Cellular and Microenvironmental Multidrug Resistance on Tumor-Targeted Drug Delivery in Triple-Negative Breast Cancer. *J. Control. Release* **2023**, *354*, 784–793. DOI: 10.1016/j.jconrel.2022.12.056.
[6] Wilczewska, A. Z.; Niemirowicz, K.; Markiewicz, K. H.; Car, H. Nanoparticles as Drug Delivery Systems. *Pharmacol. Rep.* **2012**, *64*, 1020–1037. DOI: 10.1016/S1734-1140(12)70901-5.
[7] Li, Y.; Li, N.; Pan, W.; Yu, Z.; Yang, L.; Tang, B. Hollow Mesoporous Silica Nanoparticles with Tunable Structures for Controlled Drug Delivery. *ACS Appl. Mater. Interfaces* **2017**, *9*, 2123–2129. DOI: 10.1021/acsami.6b13876.
[8] Mosseri, A.; Sanchez-Uriel, L.; Garcia-Peiro, J. I.; Hornos, F.; Hueso, J. L. A Review of Silica-Based Nanoplatforms for Anticancer Cargo Delivery. *Int. J. Mol. Sci.* **2025**, *26*, 5850. DOI: 10.3390/ijms26125850.

[9] Ranđelović, P.; Veljković, S.; Stojiljković, N.; Sokolović, D.; Ilić, I.; Laketić, D.; Randjelović, D.; Randjelović, N. The Beneficial Biological Properties of Salicylic Acid. *Acta Fac. Med. Naiss.* **2015**, *32*, 259–265. DOI: 10.1515/afmnai-2015-0026.

[10] Yin, M. J.; Yamamoto, Y.; Gaynor, R. B. The Anti-Inflammatory Agents Aspirin and Salicylate Inhibit the Activity of IκB Kinase-β. *Nature* **1998**, *396*, 77–80. DOI: 10.1038/23948.

[11] Jin, H.; Lee, Y. R.; Kim, S.; Choi, E.; Lee, K.-Y.; Joo, H. K.; Lee, E.-O.; Kim, C.-S.; Kim, J. R.; Lee, S. H.; Jeon, B. H. Synergistic Inhibition of Triple-Negative Breast Cancer by Acetylsalicylic Acid and Recombinant Human APE1/Ref-1 in a Mouse Xenograft Model. *Biomedicines* **2025**, *13*, 2767. DOI: 10.3390/biomedicines13112767.

[12] You, X.; Wang, L.; Wang, L.; Wu, J. Rebirth of Aspirin Synthesis by-Product: Prickly Poly (Salicylic Acid) Nanoparticles as Self-Anticancer Drug Carrier. *Adv. Funct. Mater.* **2021**, *31*, 2100805. DOI: 10.1002/adfm.202100805.

[13] Zhou, Y.; Chang, C.; Liu, Z.; Zhao, Q.; Xu, Q.; Li, C.; Chen, Y.; Zhang, Y.; Lu, B. Hyaluronic Acid-Functionalized Hollow Mesoporous Silica Nanoparticles as pH-Sensitive Nanocarriers for Cancer Chemo-Photodynamic Therapy. *Langmuir* **2021**, *37*, 2619–2628. DOI: 10.1021/acs.langmuir.0c03250.

[14] Cao, Y.; Wu, C.; Liu, Y.; Hu, L.; Shang, W.; Gao, Z.; Xia, N. Folate Functionalized pH-Sensitive Photothermal Therapy Traceable Hollow Mesoporous Silica Nanoparticles as a Targeted Drug Carrier to Improve the Antitumor Effect of Doxorubicin in the Hepatoma Cell Line SMMC-7721. *Drug Deliv.* **2020**, *27*, 258–268. DOI: 10.1080/10717544.2020.1718801.

[15] Slowing, I. I.; Vivero, J. L.; Escoto, C. W.; Wu, V. S.; Lin, Y. Mesoporous Silica Nanoparticles as Controlled Release Drug Delivery and Gene Transfection Carriers. *Adv. Drug Deliv. Rev.* **2008**, *60*, 1278–1288. DOI: 10.1016/j.addr.2008.03.012.

[16] Asefa, T.; Tao, Z. Biocompatibility of Mesoporous Silica Nanoparticles. *Chem. Res. Toxicol.* **2012**, *25*, 2265–2284. DOI: 10.1021/tx300166u.

[17] Mamaeva, V.; Sahlgren, C.; Lindén, M. Mesoporous Silica Nanoparticles in Medicine-Recent Advances. *Adv. Drug Deliv. Rev.* **2013**, *65*, 689–702. DOI: 10.1016/j.addr.2012.07.018.

[18] Croissant, J. G.; Fatieiev, Y.; Almalik, A.; Khashab, N. M. Mesoporous Silica and Organosilica Nanoparticles: Physical Chemistry, Biosafety, Delivery Strategies, and Biomedical Applications. *Adv. Healthc. Mater.* **2018**, *7*, 1700831. DOI: 10.1002/adhm.201700831.

[19] Vallet-Regí, M.; Balas, F.; Arcos, D. Mesoporous Materials for Drug Delivery. *Angew. Chem. Int. Ed.* **2007**, *46*, 7548–7558. DOI: 10.1002/anie.200604488.

[20] Chandran, K.; Shane, D. I.; Zochedh, A.; Sultan, A. B.; Kathiresan, T. Docking Simulation and ADMET Prediction-Based Investigation on the Phytochemical Constituents of Noni (*Morinda citrifolia*) Fruit as a Potential Anticancer Drug. *In Silico Pharmacol.* **2022**, *10*, 14. DOI: 10.1007/s40203-022-00130-4.

[21] Zochedh, A.; Chandran, K.; Priya, M.; Sultan, A. B.; Kathiresan, T. Molecular Simulation of Naringin Combined with Experimental Elucidation–Pharmaceutical Activity and Molecular Docking against Breast Cancer. *J. Mol. Struct.* **2023**, *1285*, 135403. DOI: 10.1016/j.molstruc.2023.135403.

[22] Mohan Viswanathan, T.; Krishnakumar, V.; Senthilkumar, D.; Chitradevi, K.; Vijayabhaskar, R.; Rajesh Kannan, V.; Senthil Kumar, N.; Sundar, K.; Kunjiappan, S.; Babkiewicz, E.; et al. Combinatorial Delivery of Gallium (III) Nitrate and Curcumin Complex-Loaded Hollow Mesoporous Silica Nanoparticles for Breast Cancer Treatment. *Nanomaterials* **2022**, *12*, 1472. DOI: 10.3390/nano12091472.

[23] Chen, F.; Hong, H.; Shi, S.; Goel, S.; Valdovinos, H. F.; Hernandez, R.; Theuer, C. P.; Barnhart, T. E.; Cai, W. Engineering of Hollow Mesoporous Silica Nanoparticles for Remarkably Enhanced Tumor Active Targeting Efficacy. *Sci. Rep.* **2014**, *4*, 5080. DOI: 10.1038/srep05080.

[24] Meftah, N.; Hani, A.; Merdas, A. Extraction and Physicochemical Characterization of Highly-Pure Amorphous Silica Nanoparticles from Locally Available Dunes Sand. *Chem. Africa* **2023**, *6*, 3039–3048. DOI: 10.1007/s42250-023-00688-2.

[25] Zhang, W.; Liu, H.; Qiu, X.; Zuo, F.; Wang, B. Mesoporous Silica Nanoparticles as a Drug Delivery Mechanism. *Open Life Sci.* **2024**, *19*, 20220867. DOI: 10.1515/biol-2022-0867.

[26] Güncüm, E.; Işıklan, N.; Anlaş, C.; Ünal, N.; Bulut, E.; Bakırel, T. Development and Characterization of Polymeric-Based Nanoparticles for Sustained Release of Amoxicillin–An Antimicrobial Drug. *Artif. Cells. Nanomed. Biotechnol.* **2018**, *46*, 964–973. DOI: 10.1080/21691401.2018.1476371.

[27] Bavnhøj, C. G.; Knopp, M. M.; Löbmann, K. Effect of Drug Loading in Mesoporous Silica on Amorphous Stability and Performance. *Pharmaceutics* **2024**, *16*, 163. DOI: 10.3390/pharmaceutics16020163.

[28] Huang, L.; Liu, J.; Gao, F.; Cheng, Q.; Lu, B.; Zheng, H.; Xu, H.; Xu, P.; Zhang, X.; Zeng, X. A Dual-Responsive, Hyaluronic Acid Targeted Drug Delivery System Based on Hollow Mesoporous Silica Nanoparticles for Cancer Therapy. *J. Mater. Chem. B* **2018**, *6*, 4618–4629. DOI: 10.1039/C8TB00989A.

[29] Chen, Z.; Wan, L.; Yuan, Y.; Kuang, Y.; Xu, X.; Liao, T.; Liu, J.; Xu, Z. Q.; Jiang, B.; Li, C. pH/GSH-Dual-Sensitive Hollow Mesoporous Silica Nanoparticle-Based Drug Delivery System for Targeted Cancer Therapy. *ACS Biomater. Sci. Eng.* **2020**, *6*, 3375–3387. DOI: 10.1021/acsbiomaterials.0c00073.

[30] He, Y.; Shao, L.; Usman, I.; Hu, Y.; Pan, A.; Liang, S.; Xu, H. A pH-Responsive Dissociable Mesoporous Silica-Based Nanoplatform Enabling Efficient Dual-Drug Co-delivery and Rapid Clearance for Cancer Therapy. *Biomater. Sci.* **2020**, *8*, 3418–3429. DOI: 10.1039/D0BM00204F.

[31] Jafari, S.; Soleimani, M.; Badinezhad, M. Application of Different Mathematical Models for Further Investigation of *In Vitro* Drug Release Mechanisms Based on Magnetic Nano-Composite. *Polym. Bull.* **2022**, *79*, 1021–1038. DOI: 10.1007/s00289-021-03537-9.

[32] Poór, P.; Takács, Z.; Béla, K.; Czékus, Z.; Szalai, G.; Tari, I. Ethylene Signaling in Salt Stress- and Salicylic Acid-Induced Programmed Cell Death in Tomato Suspension Cells. *Protoplasma* **2013**, *250*, 273–284. DOI: 10.1007/s00709-012-0408-4.

[33] Yin, H.; Yan, Q.; Liu, Y.; Yang, L.; Liu, Y.; Luo, Y.; Chen, T.; Li, N.; Wu, M. Co-encapsulation of Paclitaxel and 5-Fluorouracil in Folic Acid-Modified, Lipid-Encapsulated Hollow Mesoporous Silica Nanoparticles for Synergistic Breast Cancer Treatment. *RSC Adv.* **2022**, *12*, 32534–32551. DOI: 10.1039/D2RA03718A.

[34] Kovács, J.; Poór, P.; Szepesi, Á.; Tari, I. Salicylic Acid Induced Cysteine Protease Activity during Programmed Cell Death in Tomato Plants. *Acta Biol. Hung.* **2016**, *67*, 148–158. DOI: 10.1556/018.67.2016.2.3.

[35] Nguyen Thi, N. T.; Nguyen, D. H. Hollow Mesoporous Silica Nanoparticles Fabrication for Anticancer Drug Delivery. *Vietnam J. Sci. Technol.* **2020**, *58*, 39–45. DOI: 10.15625/2525-2518/58/1/14267.

[36] Krishnan, A.; Francis, M. A. pH-Responsive Delivery of 6-Mercaptopurine-Loaded Hollow Mesoporous Silica Nanoparticles for Breast Cancer Therapy. *BioNanoScience* **2025**, *15*, 594. DOI: 10.1007/s12668-025-02237-2.

[37] Day, C. M.; Sweetman, M. J.; Song, Y.; Plush, S. E.; Garg, S. Functionalized Mesoporous Silica Nanoparticles as Delivery Systems for Doxorubicin: Drug Loading and Release. *Appl. Sci.* **2021**, *11*, 6121. DOI: 10.3390/app11136121.

[38] Viswanathan, T. M.; Chitradevi, K.; Zochedh, A.; Vijayabhaskar, R.; Sukumaran, S.; Kunjiappan, S.; Kumar, N. S.; Sundar, K.; Babkiewicz, E.; Maszczyk, P.; Kathiresan, T. Guanidine–Curcumin Complex-Loaded Amine-Functionalised Hollow Mesoporous Silica Nanoparticles for Breast

Cancer Therapy. *Cancers* **2022**, *14*, 3490. DOI: 10.3390/cancers14143490.

[39] Ekenna, I. C.; Abali, S. O. Comparison of the Use of Kinetic Model Plots and DD Solver Software to Evaluate the Drug Release from Griseofulvin Tablets. *J. Drug Deliv. Ther.* **2022**, *12*, 5–13. DOI: 10.22270/jddt.v12i2-S.5402.

[40] Yi, Y. W.; Hong, W.; Kang, H. J.; Kim, H. J.; Zhao, W.; Wang, A.; Seong, Y. S.; Bae, I. Inhibition of the PI 3K/AKT Pathway Potentiates Cytotoxicity of EGFR Kinase Inhibitors in Triple-Negative Breast Cancer Cells. *J. Cell. Mol. Med.* **2013**, *17*, 648–656. DOI: 10.1111/jcmm.12046.

[41] Pal, A.; Tapadar, P.; Pal, R. Exploring the Molecular Mechanism of Cinnamic Acid-Mediated Cytotoxicity in Triple Negative MDA-MB-231 Breast Cancer Cells. *Anticancer Agents Med. Chem.* **2021**, *21*, 1141–1150. DOI: 10.2174/1871520620666200807222248.

[42] Riyasdeen, A.; Senthilkumar, R.; Periasamy, V. S.; Preethy, P.; Srinag, S.; Zeeshan, M.; Krishnamurthy, H.; Arunachalam, S.; Akbarsha, M. A. Antiproliferative and Apoptosis-Induction Studies of a Metallosurfactant in Human Breast Cancer Cell MCF-7. *RSC Adv.* **2014**, *4*, 49953–49959. DOI: 10.1039/c4ra06702a.